Materials Science and Engineering A 527 (2010) 6053–6063

Contents lists available at ScienceDirect

Materials Science and Engineering A

journal homepage: www.elsevier.com/locate/msea

Influence of heat treatment on fatigue behaviour of high-strength Mg–10Gd–3Y alloy

J. Dong[a], W.C. Liu[a,b,*], X. Song[b], P. Zhang[c], W.J. Ding[a,d], A.M. Korsunsky[b]

[a] National Engineering Research Center of Light Alloy Net Forming, School of Materials Science and Engineering, Shanghai Jiao Tong University, Shanghai 200240, China
[b] Department of Engineering Science, University of Oxford, Parks Road, Oxford OX1 3PJ, UK
[c] Physical Metallurgy and Materials Technology, Technical University of Brandenburg at Cottbus, Konrad-Wachsmann-Allee 17, 03046 Cottbus, Germany
[d] Key State Laboratory of Metal Matrix Composite, School of Materials Science and Engineering, Shanghai Jiao Tong University, Shanghai 200240, China

ARTICLE INFO

Article history:
Received 2 January 2010
Received in revised form 1 June 2010
Accepted 10 June 2010

Keywords:
Heat treatment
High cycle fatigue
Magnesium alloy
Mg–10Gd–3Y

ABSTRACT

The current work investigated the influence of heat treatment (T4, T5 and T6) on high cycle fatigue (HCF) behaviour of the as-extruded Mg–10Gd–3Y (GW103, wt.%) alloy. The five heat treatment conditions applied to the as-extruded GW103 alloy were under-aging (T5, 225 °C × 4 h), peak-aging (T5, 225 °C × 10 h), over-aging (T5, 225 °C × 250 h), solution treatment (T4, 500 °C × 4 h), solution treatment plus artificial aging (T6, 500 °C × 4 h + 225 °C × 10 h), respectively. The results showed that T5 heat treatment can improve the fatigue behaviour of the GW103 alloy, while T4 and T6 heat treatments are detrimental to the fatigue behaviour of the GW103 alloy. The 10^7 cycles fatigue strength of the GW103 alloy made by peak-aging was improved by approximately 10%, compared with the as-extruded. While, the fatigue strength of the under-aged and over-aged GW103 alloys have no obvious difference, although fatigue life of the under-aged GW103 alloy is slightly higher than that of the over-aged GW103 alloy at high stress amplitude. The extruded-T4 and extruded-T6 GW103 alloys exhibit similar fatigue strengths of 110 MPa. The influence mechanism of heat treatment on HCP behaviour of the as-extruded GW103 alloy was discussed.

1. Introduction

Magnesium alloys are very attractive candidate materials to achieve high performance and energy savings in machines and structures, because of their good specific properties, such as stiffness and strength. Magnesium alloys have recently been attracting increasing interest as candidate structural materials in many applications. In particular, they are being considered to replace aluminum alloys with a concomitant saving in weight in automotive industries [1–3]. For the applications within the load-bearing components, it is necessary to evaluate the fatigue properties of these materials [4].

It has been reported that the recently developed Mg–Gd–Y magnesium alloys showed considerable precipitation hardening, therefore exhibit higher specific strength at both room and elevated temperature and better creep resistance than conventional aluminum and magnesium alloys, including WE54 and QE22 [5–11]. Recently, it was reported that the Zn modified Mg–Gd–Y magnesium alloy had a high tensile yield strength of 430 MPa and an elongation of 12% [10]. Due to their excellent mechanical properties, Mg–Gd–Y alloys are expected to be used in future as wrought alloys. So far, many papers have been published about the precipitation hardening of Mg–Gd–Y alloys [6–12]. The precipitation sequence in the Mg–Gd–Y alloys has been clarified as: supersaturated solid solution (S.S.S.S.) $\rightarrow \beta''(D0_{19}) \rightarrow \beta'(cbco) \rightarrow \beta_1(fcc) \rightarrow \beta(fcc)$ [8]. In the peak-aged condition, the convex lens-shaped metastable β' precipitates lie on the $\{2\bar{1}\bar{1}0\}$ planes, which can effectively hinder the $\{0001\}\langle 11\bar{2}0\rangle$ basal slip [9,13].

Although it is now well established that Mg–Gd–Y series magnesium alloys can show considerable precipitation hardening, it remains unclear whether heat treatments such as T5, T4 and T6 improve or degrade the high cycle fatigue (HCF) resistance of these magnesium alloys, and which of the different aging conditions – under-aging (UA), peak-aging (PA), or over-aging (OA) – has the most beneficial effect on the HCF behaviour. The work for the 7010 aluminum alloy by Desmukh et al. [14] showed that the over-aged material exhibits higher fatigue crack growth rate, higher fatigue crack propagation threshold and higher fatigue strength corresponding to 10^6 cycles as compared to the peak-aged alloy. While for an Al–Li–Cu alloy, Jata and Starke [15] found that the general trend of increasing fatigue crack growth resistance with

* Corresponding author at: Shanghai Jiao Tong University, School of Materials Science and Engineering, 800 Dongchuan Road, Min Hang, Shanghai 200240, China. Tel.: +86 21 54742619; fax: +86 21 34202794.
E-mail address: liuwc@sjtu.edu.cn (W.C. Liu).

0921-5093/$ – see front matter © 2010 Elsevier B.V. All rights reserved.
doi:10.1016/j.msea.2010.06.030

lower aging time persists even when both crack closure and crack deflection are taken into account, i.e., that under-aged Al–Li–Cu alloy exhibits the highest fatigue crack growth resistance. However, the literatures available for magnesium alloys related to the above mentioned problems remain quite scarce to date. In order to expand their applications, it is necessary to investigate the influence of heat treatment on fatigue properties of Mg–Gd–Y alloys.

Based on the above reasons, the present study aims to investigate the influence of heat treatment on the HCF behaviour of as-extruded Mg–10Gd–3Y (GW103 alloy) at ambient temperature.

2. Experimental

The material used in this study is an Mg–10Gd–3Y (wt.%) alloy, which can be produced by permanent mold casting. Mg–25Gd (wt.%) and Mg–25Y (wt.%) master alloys were made first by melting high-purity elemental Mg (>99.95%), Gd (>99.9%) and Y (>99.9%) in a vacuum medium-frequency induction furnace under an argon atmosphere. An alloy ingot with a nominal composition of Mg–10Gd–3Y–0.5Zr (wt.%) was then prepared from high-purity Mg (99.95%), the Mg–25Gd (wt.%), Mg–25Y (wt.%) and Mg–30Zr (wt.%) master alloys in an electric resistance furnace under the mixed atmosphere of CO_2 and SF_6 with the ratio of 100:1, and cast in steel mold of ⌀ 180 mm × 250 mm. Extrusion was performed on the 20 MN maximum load compression testing machine. Before extruding, the cast ingots were firstly homogenized at 500 °C for 10 h in an electric furnace, then hot-extruded to a cylindrical bar of 50 mm in diameter at the extrusion speed of 12 mm/s after soaking at 450 °C for 2 h, with an extrusion ratio of 13. Based on the experimental results in Ref. [9], T5 (aging treatment) at 225 °C for 4 h (under-aging), 10 h (peak-aging) and 250 h (over-aging), T4 (solution treatment) at 500 °C for 4 h, T6 (solution treatment plus artificial aging) at 500 °C for 4 h followed 225 °C for 10 h were applied to five as-extruded cylindrical bars respectively. These were compared with the samples of as-extruded Mg–10Gd–3Y alloy. The GW103 alloy conditions were named extruded-F, extruded-UA, extruded-PA, extruded-OA, extruded-T4 and extruded-T6, respectively. The real chemical composition was determined to be Mg–9.86Gd–2.84Y–0.43Zr (wt.%) by an inductively coupled plasma analyzer (Perkin Elmer, Plasma-400). For the convenience in narration, the alloy studied hereinafter can be simply designated as GW103 alloy.

Specimens for mechanical testing were machined with the load axis parallel to extrusion direction (ED) of the as-extruded bars. Tensile properties of the six magnesium alloys were performed with sheet specimens with marked dimension of 15 mm gauge length, 3.6 mm width and 2 mm thickness at the initial strain rate of $5 \times 10^{-4}\ s^{-1}$.

For fatigue testing, hour-glass-shaped round specimens were used; the dimensions of the specimens were as per the instruction of the ASTM E 466 specification with a gage diameter of 5.8 mm. The machined specimens were electrolytically polished (EP) in order to avoid the influence of machining on the fatigue results.

Fatigue tests were performed under rotating beam loading ($R = -1$) at a frequency of about 100 Hz in air. To confirm whether the non-propagating cracks (NPC) may exist in the studied alloys, the coaxing effect on the fatigue limit was investigated using so called HCF step test. The term 'coaxing effect' refers to the phenomenon whereby the fatigue resistance of some metals may be improved by understressing followed by a process of gradually increasing the amplitude of the alternating stress. The coaxing effect is one of the distinctive features of the materials having a marked fatigue limit on the S–N curve and may be linked to the crack arrest behaviour. The tests were conducted on fatigue specimens in the regime that if no failure occurred after 10^7 cycles, the maximum stress level was successively increased by 5 MPa until specimen failure occurred [16].

Crack initiation and propagation behaviour during fatigue was investigated by combining direct observation of the specimen surface and the replica method using optical microscope (OM) at 400× magnification. Alloy etching was performed with a mixture of 5 g picric acid + 5 g acetic acid + 100 ml ethyl alcohol for microstructure observation by OM. In order to examine the interaction between crack initiation and propagation, on one hand, and the microstructure of the specimen, on the other hand, the fatigue experiment was conducted on the specimens whose microstructure was pre-revealed by etching.

Phase composition was characterized by X-ray diffraction using Ni-filtered Cu-Kα radiation. The microstructures and fatigue fracture surfaces of the investigated alloys were observed respectively using OM and scanning electron microscopy (SEM, Philip-505).

3. Results

3.1. Microstructure and mechanical properties

The microstructures of GW103 alloy in different conditions are shown in Fig. 1. For extruded-F and three aging-treated GW103 alloys, as seen from Fig. 1(a, c, e, and g), the microstructures of longitudinal sections consist of banded microstructures of Regions A, B and C that are typical characteristics of deformation structures, these regions appear as parallel layers and clearly mark out the deformation flow-lines [4,17,18]. Regions A, B and C correspond to the banded microstructure (not fully recrystallized elongated α-Mg grains), Mg-base solid solution (α-Mg grains, about 11 μm) and precipitates (MgGdY metallic compounds), respectively. The microhardnesses for the Regions A, B and C in these alloys were measured at a very low load of 0.98 N (100 gf). The results are listed in Table 1. As seen from Table 1, the microhardnesses of the alloys on all conditions studied (extruded-F, extruded-UA, extruded-PA and extruded-OA) all show a progressive increase between Regions A, B and C. Comparatively, the microhardnesses of extruded-UA and extruded-PA in any region are superior to those of extruded-F and extruded-OA. Extruded-F alloy exhibits the lowest microhardness in any region, while extruded-OA hardness is intermediate. It is apparent from the microscopic images of the longitudinal sections and transverse sections that the precipitates are more numerous and become more homogeneously distributed with the increasing aging at 225 °C. The widths of Region C in the microscopic images of the longitudinal sections (see Fig. 1(a, c, e, and g)) for extruded-F, extruded-UA, extruded-PA and extruded-OA alloys are about 8, 11, 13 and 15 μm respectively, and also increase with the aging time. However, the size of the MgGdY metallic compounds in Region C remains stable during aging at 225 °C due to its high melting point [9].

The microstructures of the T4 and T6 treated GW103 are shown in Fig. 1(i) and (j), respectively. It can be seen that almost small precipitates observed in the extruded-F and three aging-treated conditions were redissolved into the matrix. The average grain sizes are about 63 μm in both extruded-T4 and extruded-T6 alloy con-

Table 1
The microhardnesses of deformation structures in studied GW103 alloys.

Material	Region		
	A	B	C
Extruded-F	104	108	117
Extruded-UA	130	137	157
Extruded-PA	132	140	160
Extruded-OA	115	123	144

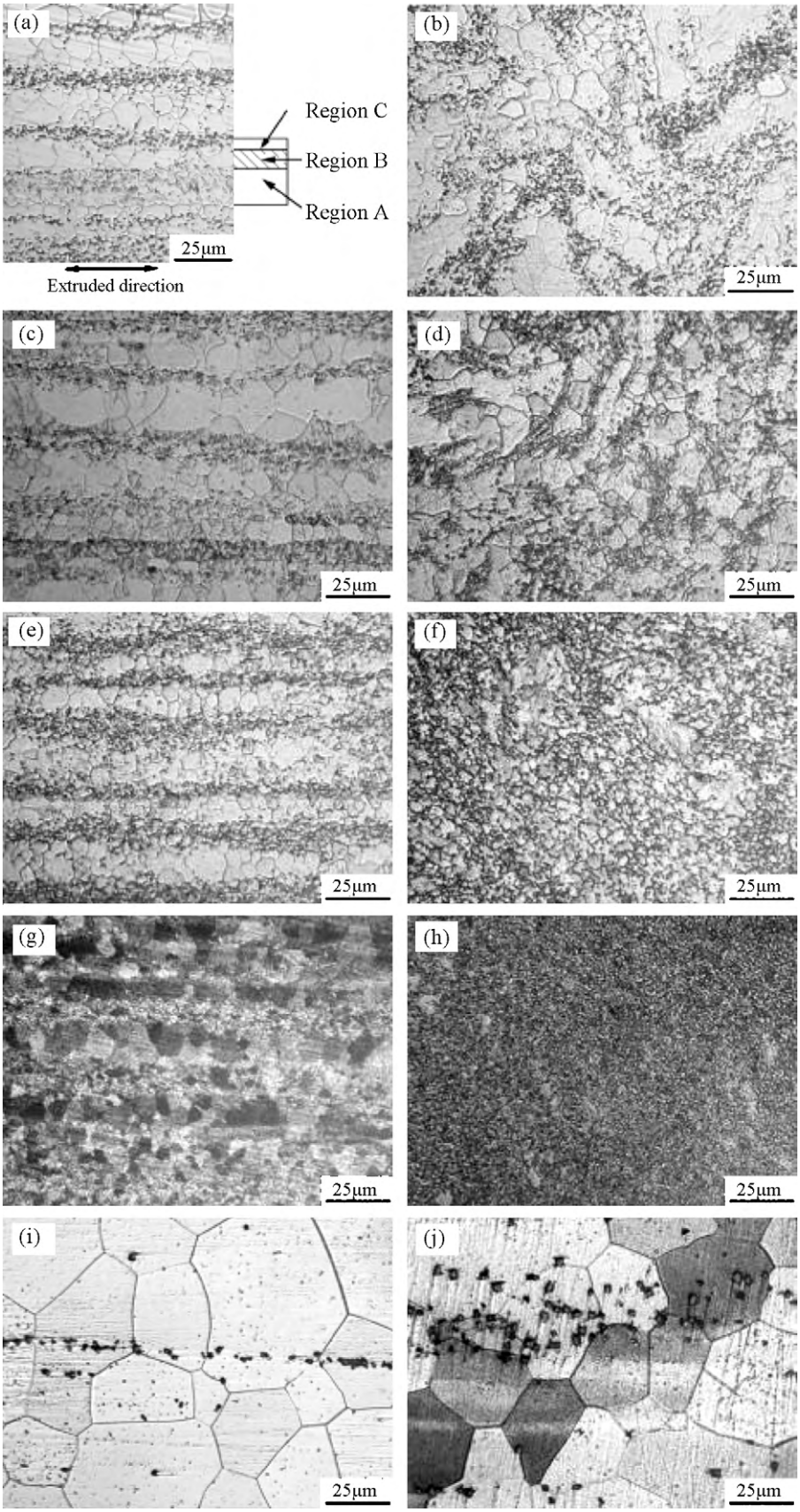

Fig. 1. Microstructure of GW103 alloy under different conditions: (a) extruded-F, longitudinal section; (b) extruded-F, transverse section; (c) extruded-UA, longitudinal section; (d) extruded-UA, transverse section; (e) extruded-PA, longitudinal section; (f) extruded-PA, transverse section; (g) extruded-OA, longitudinal section; (h) extruded-OA, transverse section; (i) extruded-T4, longitudinal section and (j) extruded-T6, longitudinal section.

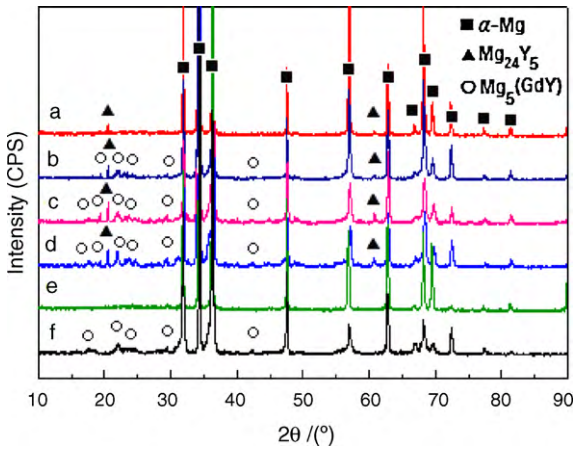

Fig. 2. XRD analysis of GW103 alloy under different conditions: (a) extruded-F; (b) extruded-UA; (c) extruded-PA; (d) extruded-OA; (e) extruded-T4 and (f) extruded-T6.

Table 2
Tensile results of the studied GW103 alloys.

Material	YS (MPa)		UTS (MPa)		EL (%)	
	$\bar{\nu}$	S	$\bar{\nu}$	S	$\bar{\nu}$	S
Extruded-F	265	2.3	344	5.2	20.9	1.8
Extruded-UA	316	3.7	408	6.1	15.3	2.1
Extruded-PA	339	4.9	445	5.3	9.1	1.3
Extruded-OA	325	5.2	409	3.8	14.7	1.3
Extruded-T4	192	2.2	286	7.7	13.5	0.8
Extruded-T6	259	5.3	388	3.9	1.5	0.5

$\bar{\nu}$ and S refer to average and standard deviation respectively.

ditions, indicating that grain growth took place during the solution treatment.

Fig. 2 shows the X-ray diffraction patterns of the GW103 alloy under different conditions. It can be observed that the extruded-F GW103 alloy is mainly composed of α-Mg solid solution and the $Mg_{24}Y_5$ secondary phase, where Gd probably substitutes Y. In aging-treated GW103 alloys illustrated in Fig. 2(b–d) [9,19], there are Mg_5 (GdY) precipitates besides α-Mg and $Mg_{24}Y_5$ intermetallics, and the Mg_5 (GdY) precipitates increase in number with the aging time. In addition, it can be seen that extruded-T4 is mainly composed of supersaturated α-Mg solid solution. There are Mg_5 (GdY) precipitates besides α-Mg present in the extruded-T6 alloy.

A comparison of the tensile properties of GW103 alloy under different conditions is presented in Table 2. As seen from Table 2, GW103 alloy is a strongly precipitation-hardened alloy [8,10]. It is clear that the T5 heat treatment can improve markedly the tensile strength of GW103 alloy, at the expense of decreased ductility. Namely, the extruded-PA GW103 alloy exhibits the highest tensile yield strength and UTS of 339 MPa and 445 MPa and the lowest elongation to failure of 9.1% among the four alloys studied. The extruded-UA and extruded-OA GW103 alloys exhibit similar tensile properties. However, solution treatment is detrimental to the tensile properties of the as-extruded GW103 alloy, i.e., the extruded-T4 GW103 alloy exhibits the lowest tensile strength compared with the aging-treated GW103.

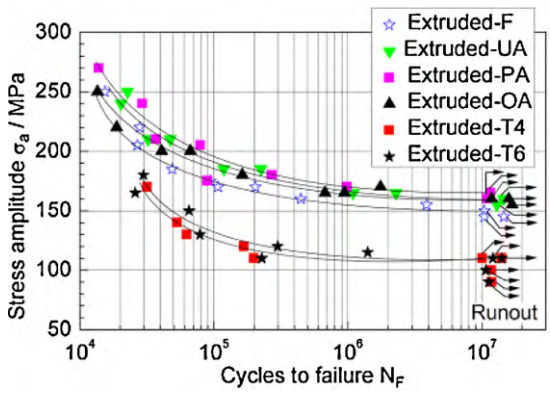

Fig. 3. S–N curves of GW103 alloy in various conditions under rotating beam loading in air ($R = -1$).

3.2. High cycle fatigue properties

For the six magnesium alloys studied, the S–N curves under rotating beam loading ($R = -1$) at a frequency of about 100 Hz in air are presented in Fig. 3. The fatigue strength (at 10^7 cycles) is listed in Table 3. As seen from Fig. 3 and Table 3, it is apparent that the HCF behaviour of the aging-treated GW103 alloys is superior to that of extruded-F GW103 alloy at any stress amplitude. Comparatively, among the three aging-treated GW103 alloys, the extruded-PA alloy shows the highest fatigue strength of 165 MPa and fatigue life at any stress amplitude, while the extruded-UA and extruded-OA alloys exhibit similar fatigue strengths of 160 MPa, with the fatigue life of the extruded-UA alloy being slightly higher than that of extruded-OA alloy at high stress amplitude. However, the solution treatment decreases the fatigue resistance of the as-extruded GW103 alloy, while the extruded-T4 and extruded-T6 alloys exhibit similar fatigue strengths that are inferior to that of the extruded-F GW103 alloy at any stress amplitude. In addition, the values of the fatigue ratio (σ_a/σ_b) for the investigated alloys are about 0.44, 0.39, 0.37, 0.39, 0.38 and 0.28, respectively, in agreement with the value for magnesium (0.25–0.5) reported in literature [3]. Comparatively, the fatigue strength of 150 MPa for the extruded-F GW103 alloy is about 50% and 7% higher than those of the high-strength wrought magnesium alloys AZ80 and ZK60, respectively [4,20]. Also, the fatigue strength improvement (15 MPa) of GW103 alloy induced by the aging treatment is slightly higher than that of ZK60 alloy (10 MPa).

3.3. Fractography

The fracture surfaces of the fatigue specimens are shown in Figs. 4–7. In the extruded-F and the three aging-treated GW103 specimens, surface crack nucleation was observed (see Figs. 4 and 5), since the surface experienced the maximum tensile stress during rotating beam loading fatigue. Nevertheless, in the extruded-T4 and extruded-T6 GW103 specimens, fatigue cracks initiate at porosities or inclusions that lie subsurface. As far as the overall fracture surface is concerned, significant differences are observed between the macroscopic fractures of the GW103 alloys after different heat treatment conditions. Compared with the extruded-F and the three aging-treated GW103 alloys, the frac-

Table 3
Fatigue strengths of the studied GW103 alloys.

Materials	Extruded-F	Extruded-UA	Extruded-PA	Extruded-OA	Extruded-T4	Extruded-T6
σ_a (MPa)	150	160	165	160	110	110
σ_a/σ_b	0.44	0.39	0.37	0.39	0.38	0.28

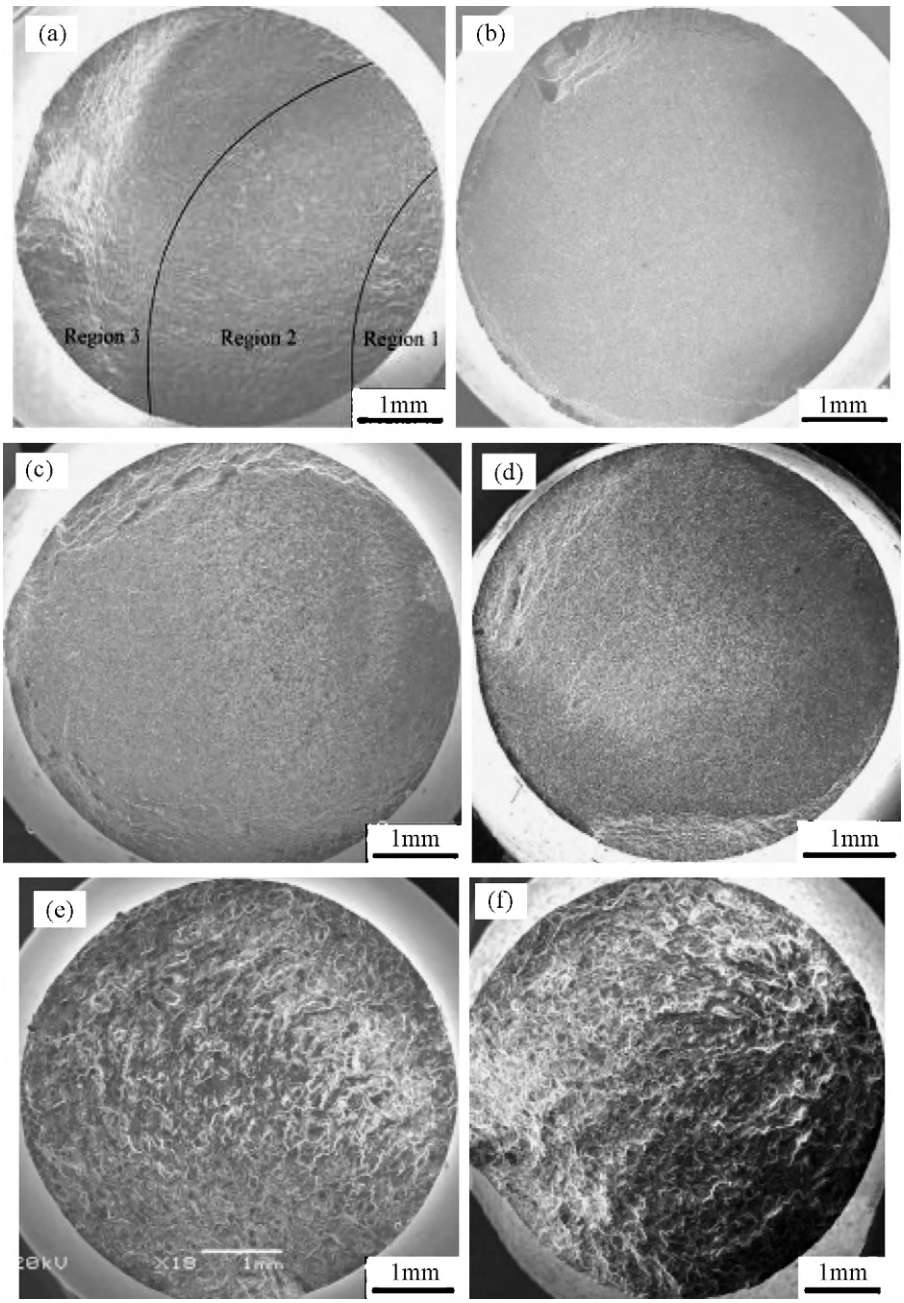

Fig. 4. Overall fracture surfaces of the studied GW103 alloys: (a) extruded-F, 155 MPa; (b) extruded-UA, 180 MPa; (c) extruded-PA, 170 MPa; (d) extruded-OA, 165 MPa; (e) extruded-T4, 130 MPa and (f) extruded-T6, 130 MPa.

ture surfaces of the extruded-T4 and extruded-T6 GW103 alloys are rougher because of their larger grain size. Among the extruded-F and the three aging-treated GW103 alloys, the extruded-F GW103 alloy displays a rougher fracture surface, and a significant zone of localized deformation is apparent. In comparison, the three aging-treated GW103 alloys have fracture surfaces that are macroscopically relatively flat.

Overall, the fracture surfaces of the studied GW103 alloy fatigue specimens display three distinct regions (see Fig. 4): the fatigue crack initiation region (Region 1), steady crack propagation region (Region 2) and the collapse fracture region (Region 3). In Region 1, it can be seen that fatigue cracks in the extruded-T4 and extruded-T6 GW103 alloys initiate subsurface at pores or inclusions, such as oxides, and that their initiation zones are obviously larger than those of the extruded-F and the three aging-treated GW103 alloys. Large inclusions have a tendency to form cracks earlier due to the more widespread plasticity surrounding them, and also promote larger initial crack size at the onset of propagation. Porosity and oxide inclusions both serve as preferential sites for fatigue crack formation. However, for the extruded-F and the three aging-treated GW103 alloys, the initiation zone in the extruded-F GW103 alloy is slightly larger than those of the three aging-treated GW103 alloys with low ductility (low elongation), indicating that the plastic zone at the fatigue crack tip of the extruded-F GW103 alloy is also larger than for the three aging-treated GW103 alloys. In Region 2, as seen from Figs. 4 and 6, the fracture surfaces of the extruded-F, aging-treated and extruded-T4 GW103 alloys demonstrate quasi-cleavage fracture characteristics. Finally, the fracture surface of the extruded-T6 GW103 alloy shows typical brittle fracture characteristic, displaying numerous cleavage planes. In addition, in

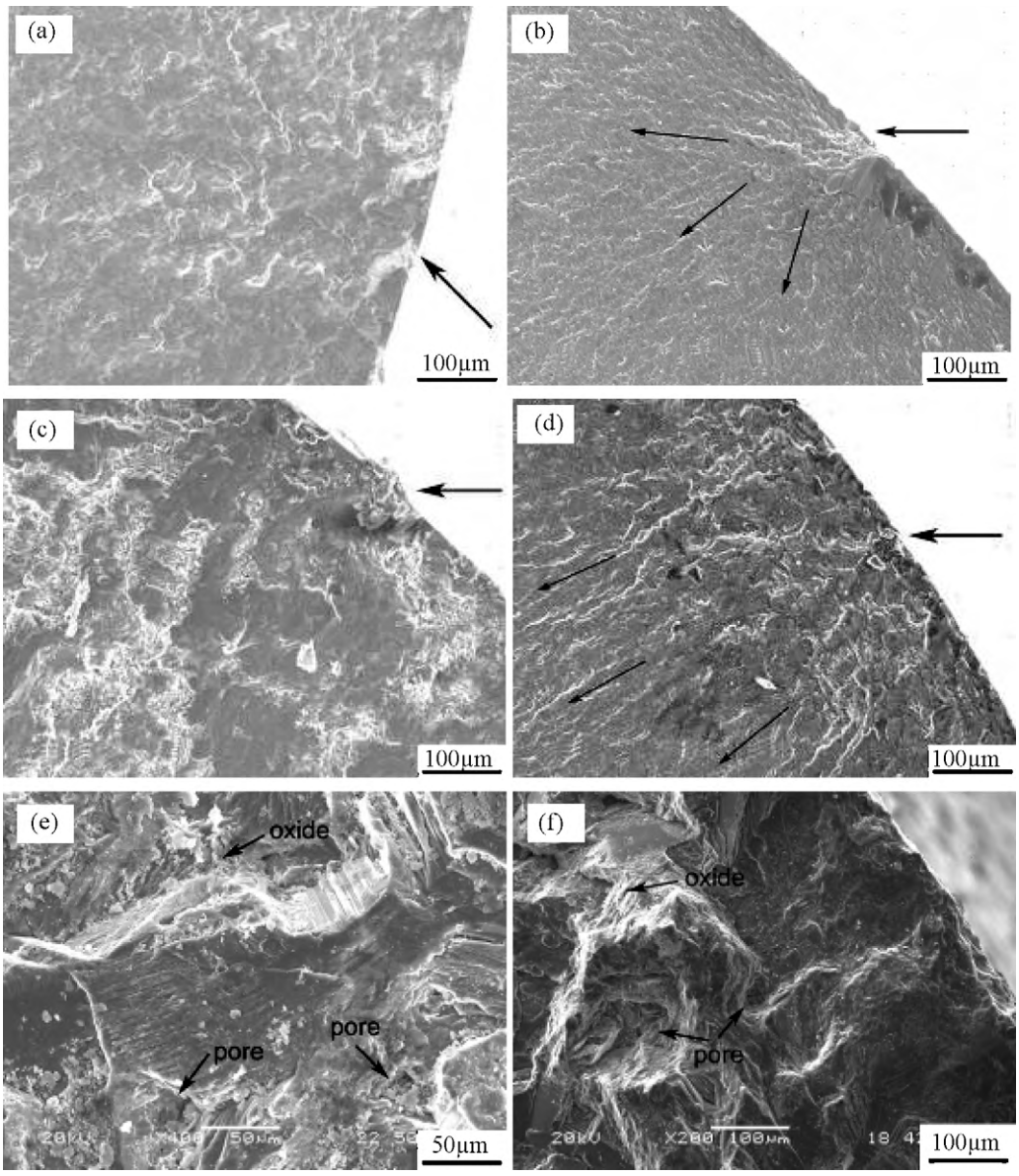

Fig. 5. Fatigue crack initiation sites from Fig. 4 of the studied GW103 alloys: (a) extruded-F; (b) extruded-UA; (c) extruded-PA; (d) extruded-OA; (e) extruded-T4 and (f) extruded-T6 (fine arrows in (b) and (d) indicate crack propagation direction).

comparison with the extruded-F GW103 alloy, the fracture surfaces of the three aging-treated GW103 alloys in Region 2 are more flat than those of the extruded-F GW103 alloy, and display fewer cleavage planes, dimples and tear ridges.

Compared with the Regions 1 and 2, Region 3 plays a minor role in determining the fatigue life (see Fig. 7). The fracture surfaces of the extruded-F and the different aging-treated GW103 alloys consist of multiple small dimples with particles inside [4]. However, in comparison with the extruded-F GW103 alloy, the fracture surfaces of these aging-treated GW103 alloys in Region 3 have fewer and shallower dimples indicating its ductility [21]. No dimples are observed in Region 3 of the extruded-T4 and extruded-T6 GW103 alloys, while numerous secondary cracks are found.

The crack initiation sites in the extruded-F (at 185 MPa), extruded-UA (at 190 MPa), extruded-PA (at 205 MPa) and extruded-OA (at 190 MPa) GW103 alloys are shown in Fig. 8. In the Figure, the arrows indicate the crack tips. It can be seen that the cracks in the four specimens initiated in Region B, indicating that the matrix with higher strength and elongation to fracture exhibits higher crack initiation life and fatigue strength. In addition, it should be noted that the fatigue cracks in the extruded-T4 and extruded-T6 alloys mainly initiate subsurface and thus the crack initiation cannot be observed by means of replication.

Fig. 9 shows the small crack growth paths in the investigated alloys. As seen in Fig. 9, for the extruded-F and aging-treated GW103 alloys, the crack paths in Regions A and C are straight, while the crack paths in Region B have a zigzag characteristic and represent a mixed mode between transgranular and intergranular fracture. Specifically, the cracks pass through large grain (solid solution) and bypass small grain. Compared to the aging-treated GW103 alloys (see Fig. 9(b–d)), the crack path in the extruded-F GW103 alloy is more tortuous and even induces secondary cracks and multiple cracking (see Fig. 9(a)). This indicates that the extruded-F GW103 alloy possesses higher crack growth resistance. In addition, as seen from Fig. 9(e and f), though the extruded-T4 and extruded-T6 GW103 alloys also display a mixture of transgranular and intergranular fracture, there is a difference between the extruded-T4 and extruded-T6 alloys, i.e., the extruded-T4

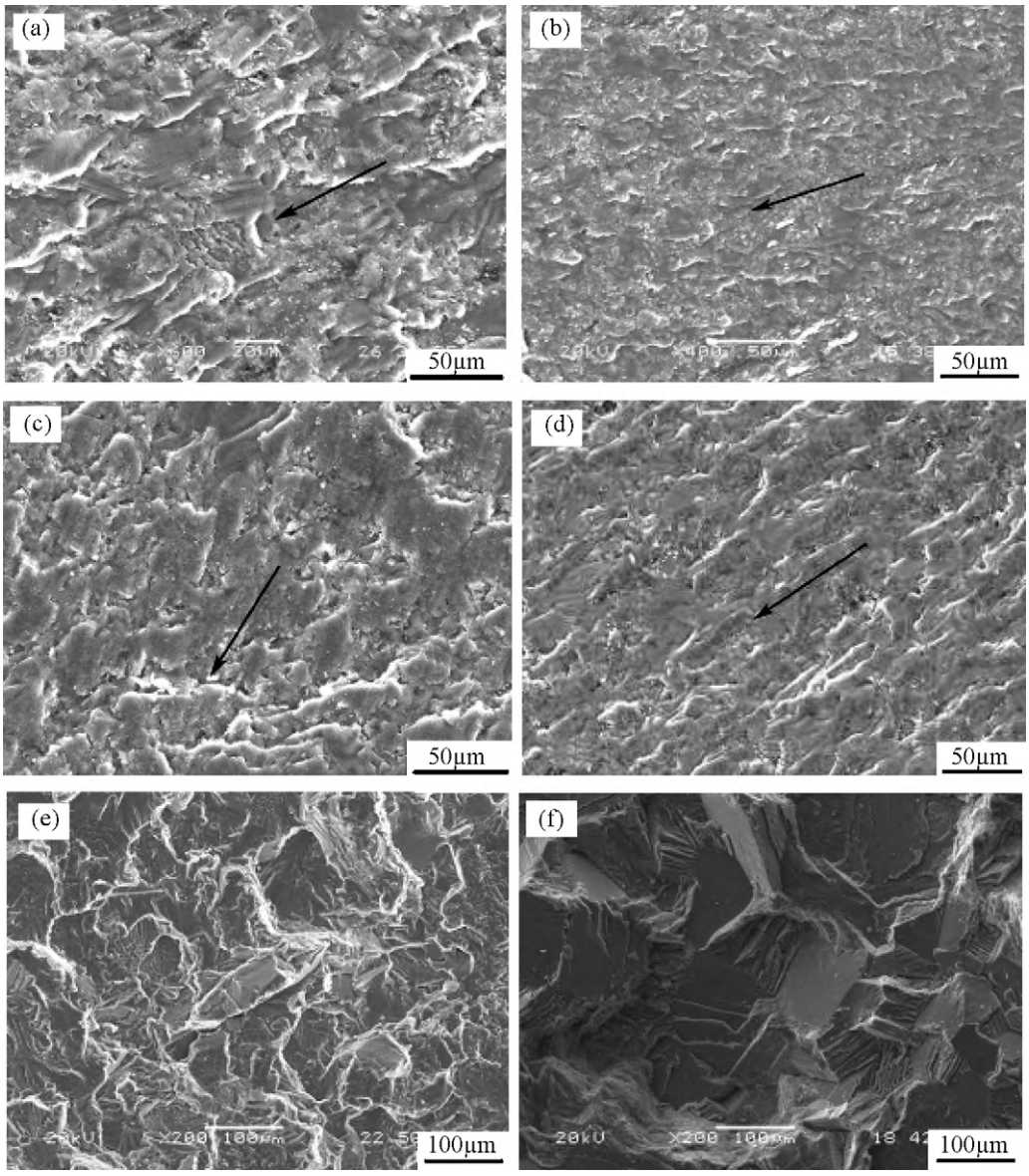

Fig. 6. SEM images from Region 2 in Fig. 4 of the investigated GW103 alloys: (a) extruded-F; (b) extruded-UA; (c) extruded-PA; (d) extruded-OA; (e) extruded-T4 and (f) extruded-T6 (fine arrows in (a), (b), (c) and (d) indicate crack propagation direction).

GW103 alloy shows mainly transgranular crack propagation and the extruded-T6 GW103 alloy shows mainly intergranular crack propagation.

4. Discussion

Generally, the fatigue strength of the as-cast magnesium alloy is determined by the existence of NPC caused by casting porosities or inclusions [22]. The term 'non-propagating crack' is that when a specimen with a sharp notch is subjected to a alternating load of moderate magnitude, there are occasions when the developed crack does not propagate itself further unless the load on the specimen is increased, although the fatigue crack has developed at the root of the notch. It does not cause component failure. In contrast, the fatigue strength of wrought magnesium alloys is mainly determined by (1) the existence of NPC caused by the grain boundaries of metallic compounds [18], (2) crack initiation [23]. For the GW103 alloy studied in this work, grain growth is obvious after T4 solution treatment, with the secondary phase $Mg_{24}Y_5$ dissolving back into the α-Mg matrix and turning into a supersaturated solid solution. Thus, the solution treatment reduces and even eliminates the original precipitation strengthening effect during casting and the fine grain strengthening effect induced by extrusion. The fatigue strength is determined by the existence of NPC caused by casting porosities or inclusions. Therefore, the fatigue strength of the extruded-T4 alloy is inferior to that of the extruded-F alloy. Although the subsequent aging treatment can improve the tensile strength and yield strength, it also significantly reduces the elongation, and the fatigue strength of the extruded-T6 alloy shows no obvious improvement compared with the extruded-T4 alloy. For the extruded-F and the three aging-treated alloys, in order to confirm whether NPC exists in the experimented wrought alloys; step loading fatigue tests were performed to assess the coaxing effect in the extruded-F GW103 alloy. The result is shown in Fig. 10. The figure shows that no coaxing effect is observed in the extruded-F GW103 alloy, with the specimen fracturing at 155 MPa. Since the presence of coaxing effect is connected with the existence of NPC [16], the lack of coaxing effect indicates that there is no NPC in the extruded-F GW103 alloy. Moreover, it is known that the coaxing effect is associated with dynamic strain aging

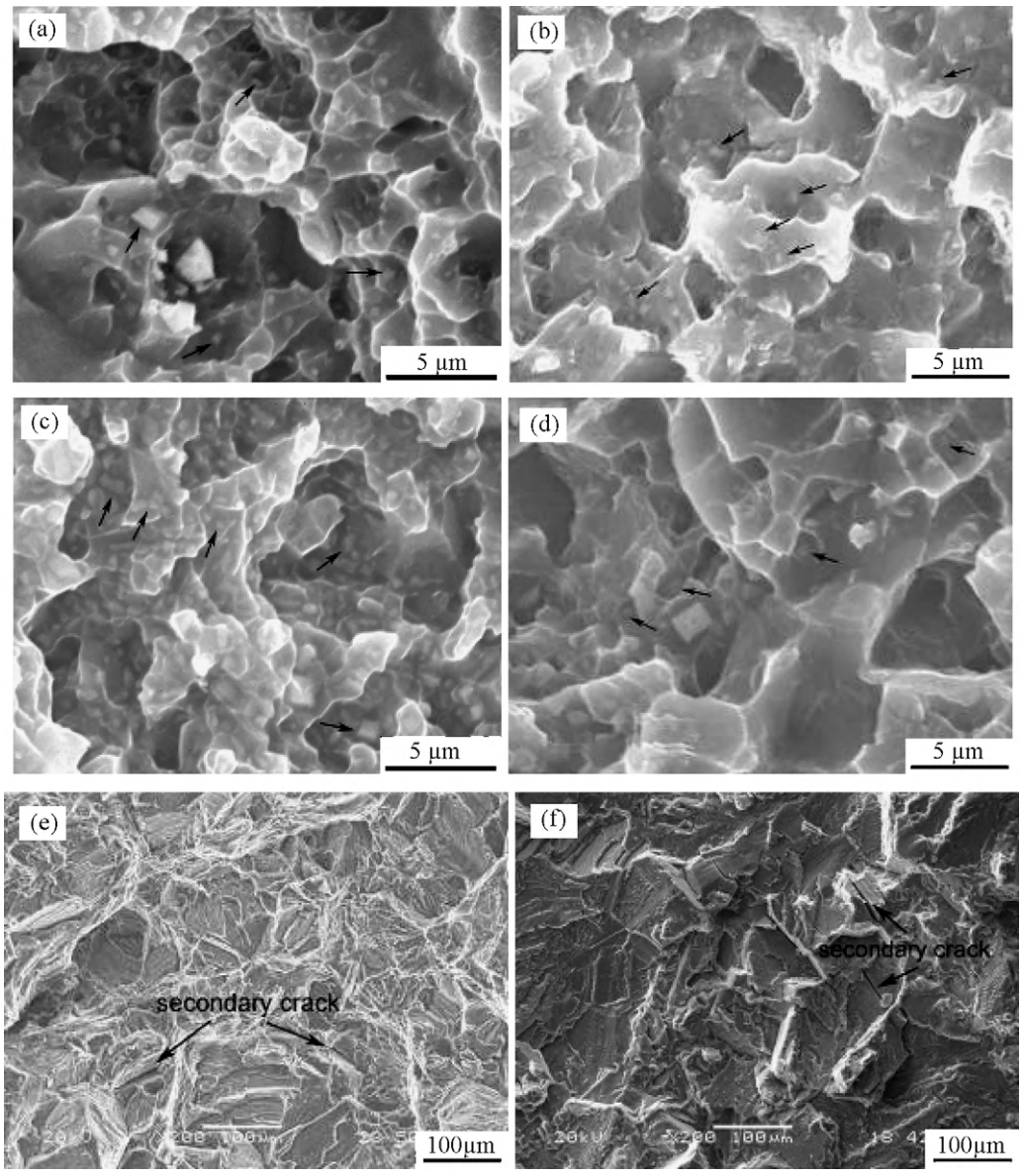

Fig. 7. SEM images from Region 3 in Fig. 4 of the investigated GW103 alloys: (a) extruded-F; (b) extruded-UA; (c) extruded-PA; (d) extruded-OA; (e) extruded-T4 and (f) extruded-T6. (the arrows in (a), (b), (c) and (d) indicate precipitates).

followed by the cyclic deformation [24]. The absence of coaxing effect implies that dynamic strain aging does not occur during fatigue, although the alloy is supersaturated with Gd and Y atoms. Therefore, the fatigue strength of the as-extruded GW103 alloy is determined by crack initiation rather than by NPC. It can be presumed that fatigue cracks will mainly nucleate at slip bands in the GW103 alloy [21,2]. Accordingly, a threshold stress for dislocation slip should exist. This threshold stress determines the stress amplitude that is necessary for the formation of slip bands and thus governs the resistance to fatigue crack nucleation of this alloy.

At room temperature, the active dislocation slip system in magnesium is the $\{0001\}\langle 11\bar{2}0\rangle$ dislocation slip system, whose critical resolved shear stress (CRSS) for pure magnesium is only about 0.51 MPa [21,25]. In contrast, non-basal slip systems such as $\{10\bar{1}0\}\langle 11\bar{2}0\rangle$ and $\{11\bar{2}2\}\langle 11\bar{2}3\rangle$ are very difficult to activate since the CRSS for non-basal slips is about 100 times higher than that of the basal slip [21]. An alternative deformation mode in magnesium alloys is the $\{10\bar{1}2\}\langle 10\bar{1}1\rangle$ twinning, which reorients the grains to activate the basal slip. However, such twinning is not observed in the fatigue specimens of the GW103 alloy by the OM at 400× magnification. Therefore, $\{0001\}\langle 11\bar{2}0\rangle$ basal slip system is likely to remain the most important deformation mode during the fatigue process.

The results of SEM–EDX analysis reveal that there are about 9.32 wt.% Gd and 2.56 wt.% Y in Region B (magnesium solid solution) and 25.26 wt.% Gd and 7.94 wt.% Y in Region C (MgGdY metallic compound) of the extruded-F GW103 alloy. The equilibrium solid solubility of Gd in magnesium is about 3.82 wt.% at 200 °C, decreasing rapidly with temperature [26]. Obviously, Gd is supersaturated in the magnesium solid solution within the GW103 alloy. The solute atoms could interact with dislocations and influence the threshold stress for dislocation glide [27]. At room temperature, the threshold stress in the GW103 alloy cannot be overcome by the thermal activation of dislocation motion. Therefore, the threshold stress may prohibit the $\{0001\}\langle 11\bar{2}0\rangle$ basal slip, leading to the appearance of a threshold level for fatigue crack initiation.

On the other hand, the GW103 alloy is a precipitation-hardened alloy [5–11]. The precipitation sequence consists of the following steps: α-Mg supersaturated solid solution (S.S.S.S.)

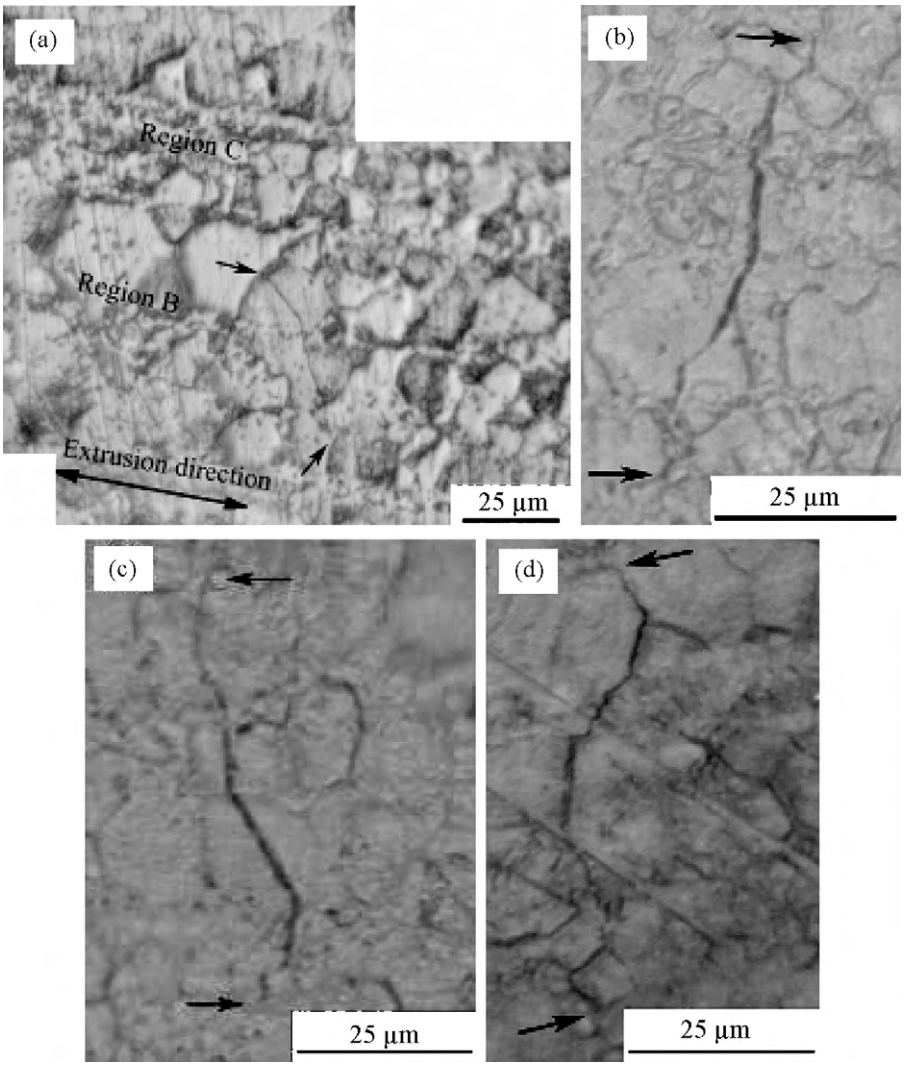

Fig. 8. Crack initiation sites on the specimen surface of the investigated alloys: (a) extruded-F, 185 MPa, $N/N_f = 0.09$; (b) extruded-UA, 190 MPa, $N/N_f = 0.64$; (c) extruded-PA, 205 MPa, $N/N_f = 0.74$ and (d) extruded-OA, 190 MPa, $N/N_f = 0.59$.

$\rightarrow$ metastable $\beta''(D0_{19}) \rightarrow$ metastable $\beta'(cbco) \rightarrow$ metastable $\beta_1(fcc) \rightarrow$ stable$\beta(fcc)$ [8]. The convex lens-shaped precipitate lies on the $\{2\bar{1}\bar{1}0\}$ planes, and can effectively hinder the $\{0001\}\langle 11\bar{2}0\rangle$ basal slip in magnesium [9,13]. The microstructure observation by OM and SEM shows that precipitation occurs along grain boundaries during the extrusion process (see Fig. 1). Obviously, precipitation could also occur inside the grains. The small precipitates could pin dislocations, resulting in the additional increase of the threshold stress for basal slip.

As discussed above, the fatigue strength in the GW103 alloy is determined by the threshold stress for basal slip, which is affected by the solid solution hardening and precipitation hardening effects.

In this study, the actual dislocation density was not measured. However, it is believed that the density of dislocations and twins are high in the extruded-F GW103 alloy, and the dislocations and twins act as precipitation nuclei during T5 heat treatment. Zheng et al. [28] investigated the effect of pre-deformation on the aging characteristics in the cast Mg–Gd–Nd–Zr alloy, and found that dislocations could indeed act as precipitation nuclei. Jin-feng et al. [29] reported that hot extrusion of spray-formed AZ91 followed by aging at 175 °C resulted in dense distributions of $Mg_{17}Al_{12}$ precipitates within grains. The precipitate density of Mg_5 (GdY) and $Mg_{24}Y_5$ in the aging-treated GW103 alloys should also increase with the aging time at 225 °C (see Fig. 1). Since dislocations mainly move on basal planes that have lower slip resistance, the precipitates in the Mg matrix act as predominant barriers to dislocation movement. Secondly, as seen from Table 1, the aging-treated GW103 alloys exhibit higher microhardness in Regions A, B and C, compared with the extruded-F GW103 alloy. Thirdly, the T5 heat treatment can also decrease residual tensile stress induced by extrusion. These effective factors will lead to higher resistance to fatigue crack initiation, namely a greater number of cycles to crack initiation and increased fatigue strength. According to Ref. [8], metastable β'' and β' phases coexist in the matrix at the under-aging stage. At the peak-aging stage, spheroidal β' precipitates form at the beginning of the steep hardness increase and then grow into prismatic plates that contribute to the hardness maximum. At the over-aging stage, the β_1 phase appears via an in situ transformation from the decomposed β' phase, although it grows in a direction that is different from that of the previous β' phase growth. Comparatively, the strengthening effect of the β' phase on fatigue crack initiation at the peak-aging stage is higher than that of the β and β_1 phases at the under-aging and over-aging stages. Therefore, compared with the three aging-treated GW103 alloys, the extruded-PA alloy shows the highest resistance to fatigue crack initiation and propagation, namely the highest fatigue strength and fatigue life, while the fatigue strength and fatigue life of the extruded-UA and extruded-OA alloys show no obvious difference.

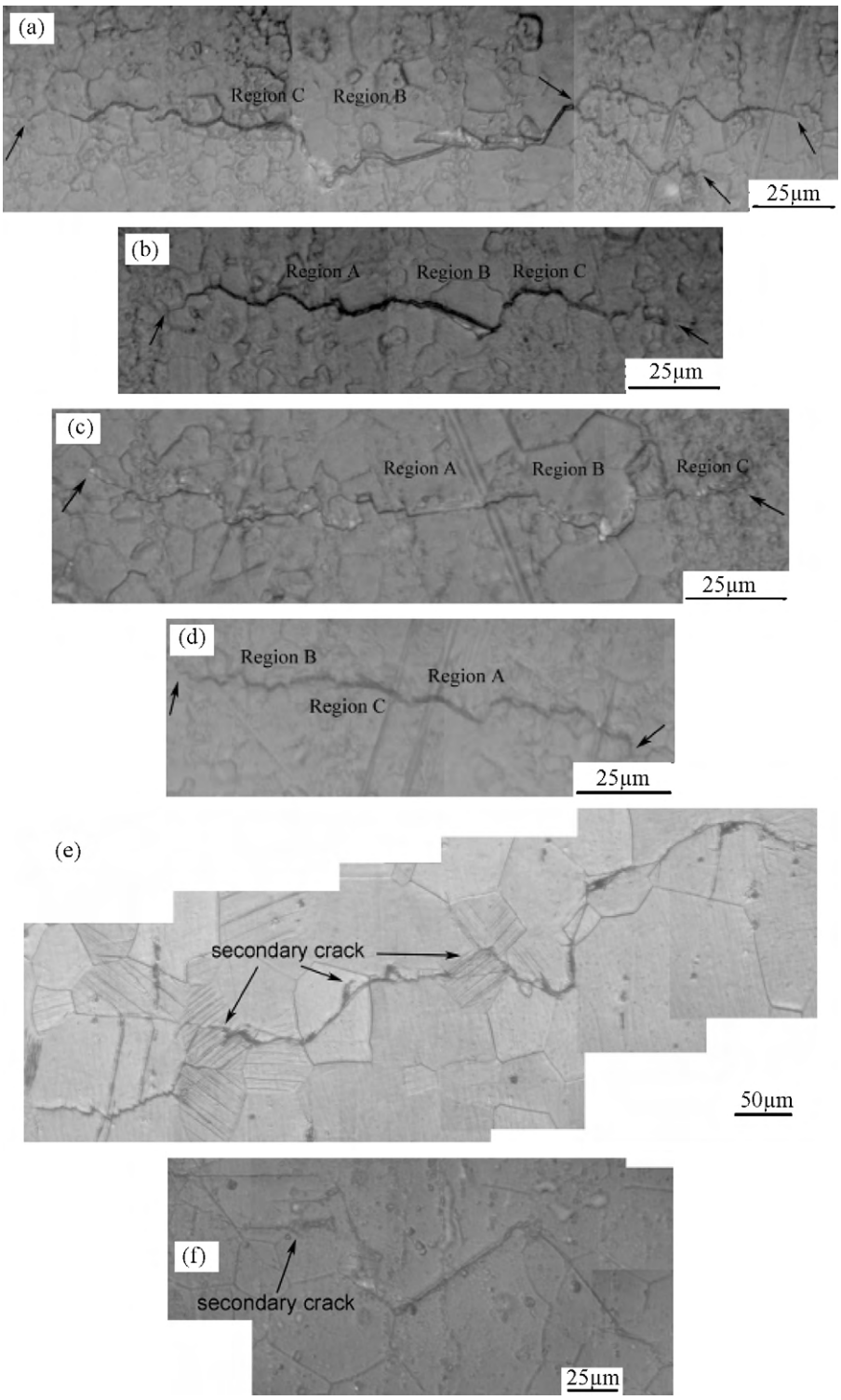

Fig. 9. Small crack growth path in the investigated alloys: (a) extruded-F, 185 MPa, $N/N_f = 0.54$; (b) extruded-UA, 210 MPa, $N/N_f = 0.89$; (c) extruded-PA, 205 MPa, $N/N_f = 0.82$; (d) extruded-OA, 190 MPa, $N/N_f = 0.71$; (e) extruded-T4, 130 MPa, $N/N_f = 0.84$ and (f) extruded-T6, 130 MPa, $N/N_f = 0.81$.

For the extruded-F GW103 alloy, the $\{0\,0\,0\,1\}\langle 1\,1\,\bar{2}\,0\rangle$ basal slip system is the most important deformation mode during fatigue loading [21]. Compared to the Mg–Al and Mg–Zn–Zr alloys such as AZ80 and ZK60 under same processing conditions [4,20], the atomic radii of Gd and Y are much larger than those of Al and Zn. Therefore, the solid solution hardening effect induced by the Gd and Y atoms in the GW103 alloy is expected to be much stronger than that of Al in Mg–Al and Zn in Mg–Zn–Zr alloys. Moreover, the precipitation hardening effect in the extruded-F GW103 alloy is also more pronounced than that in the Mg–Al and Mg–Zn–Zr alloys [21]. Precipitates of the β' phase lying on the $\{2\,1\,1\,0\}$ planes can markedly hinder the $\{0\,0\,0\,1\}\langle 1\,1\,\bar{2}\,0\rangle$ basal slip [13,9]. In contrast, the $Mg_{17}Al_{12}$ precipitates in the Mg–Al and MgZn precipitates in the Mg–Zn–Zr alloys grow along the basal planes, and are less effective as barriers for the basal slip [13,30]. This insight provides an explanation of the more significant fatigue

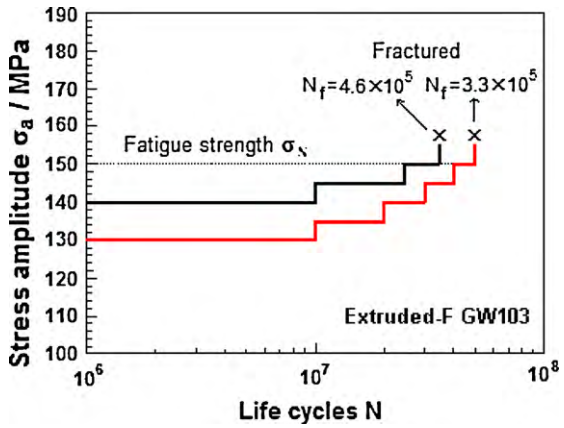

Fig. 10. Coaxing effect of extruded-F GW103 alloy.

strength increase observed in the GW103 alloy due to heat treatment.

5. Conclusions

The hot-extruded GW103 alloy was subjected to five different heat treatments, namely, under-aging, peak-aging, over-aging, T4 and T6 treatments, and compared with the hot-extruded material. High cycle fatigue behaviour of the resultant materials was investigated. The following conclusions can be drawn:

- Aging treatment can improve significantly the fatigue behaviour of the GW103 alloy. Comparatively, among the three aging-treated GW103 alloys, the fatigue strength and fatigue life of the extruded-PA alloy is the highest, while the fatigue strength and fatigue life of the extruded-UA and extruded-OA alloys are similar. However, T4 and T6 heat treatments are detrimental to the fatigue performance of the GW103 alloy, i.e., the extruded-T4 and extruded-T6 alloys present the lowest fatigue strengths of 110 MPa compared to the fatigue strengths in excess of 150 MPa for the extruded-F and the three aging-treated alloys.
- The fatigue strength improvement of the extruded-F and the aging-treated GW103 alloys mainly results from the increased threshold stress for basal slip of dislocations that is induced by the combined effect of solid solution hardening and precipitation hardening. The solid solution hardening is likely to contribute most significantly to the threshold stress, while the precipitation hardening provides a smaller additional increment.
- Fatigue cracks in the extruded-T4 and extruded-T6 GW103 alloys mainly initiate at porosities or inclusions subsurface, while fatigue cracks in the extruded-F and the three aging-treated GW103 alloys initiate in Region B at the specimen surface. Compared to the extruded-F GW103 alloy, the fatigue properties improvement of the aging-treated GW103 alloys is mainly attributed to the precipitation strengthening induced by the T5 treatment. Comparatively, the strengthening effect of the β' phase on fatigue crack initiation at the peak-aging stage is higher than that of the β and β_1 phases at the under-aging and over-aging stages.

Acknowledgments

This project is sponsored by National Natural Science Foundation of China (No. 50901045), Shanghai Rising-Star Program (A type, 09QA1403100) and the Scientific Research Foundation for the Returned Overseas Chinese Scholars, State Education Ministry, PRC.

References

[1] M.F. Horstemeyer, N. Yang, K. Gall, D.L. McDowell, J. Fan, P.M. Gullett, Acta Materialia 52 (2004) 1327–1336.
[2] K. Tokaji, M. Kamakura, Y. Ishiizumi, N. Hasegawa, International Journal of Fatigue 26 (2004) 1217–1224.
[3] V.V. Ogarevic, R.I. Stephens, Annual Review of Materials Science 20 (1990) 141–177.
[4] W.C. Liu, J. Dong, P. Zhang, Z.Y. Yao, C.Q. Zhai, W.J. Ding, Journal of Materials Science 44 (2009) 2916–2924.
[5] L.L. Rokhlin, Proceedings of N.A.T.O. Advanced Study Institute, Kluwer, 1998, pp. 443–448.
[6] I.A. Anyanwu, S. Kamado, Y. Kojima, Materials Transactions 42 (2001) 1206–1211.
[7] I.A. Anyanwu, S. Kamado, Y. Kojima, Materials Transactions 42 (2001) 1212–1218.
[8] S.M. He, X.Q. Zeng, L.M. Peng, X. Gao, J.F. Nie, W.J. Ding, Journal of Alloys and Compounds 421 (2006) 309–313.
[9] S.M. He, X.Q. Zeng, L.M. Peng, X. Gao, J.F. Nie, W.J. Ding, Journal of Alloys and Compounds 427 (2007) 316–323.
[10] T. Honma, T. Ohkubo, S. Kamado, K. Hono, Acta Materialia 55 (2007) 4137–4150.
[11] T. Honma, T. Ohkubo, K. Hono, S. Kamado, Materials Science and Engineering A 395 (2005) 301–306.
[12] G.W. Lorimer (Ed.), Proceedings Magnesium Technology, Institute of Metals, London, 1986, pp. 47–53.
[13] J.F. Nie, X. Gao, S.M. Zhu, Scripta Materialia 53 (2005) 1049–1053.
[14] M.N. Desmukh, R.K. Pandey, A.K. Mukhopadhyay, Materials Science and Engineering A 435–436 (2006) 318–326.
[15] K.V. Jata, E.A. Starke Jr., Metallurgical Transactions A 17 (1986) 1011–1026.
[16] J.H. Kim, M.G. Kim, Materials Science and Engineering A 346 (2003) 216–222.
[17] S. Ishihara, Z.Y. Nan, T. Goshima, Materials Science and Engineering A 468–470 (2007) 214–222.
[18] Z.Y. Nan, S. Ishihara, A.J. McEvily, H. Shibata, K. Komano, Scripta Materialia 56 (2007) 649–652.
[19] X.B. Liu, R.S. Chen, E.H. Han, Journal of Alloys and Compounds 465 (2008) 232–238.
[20] P. Zhang, J. Lindemann, Scripta Materialia 52 (2005) 485–490.
[21] P. Zhang, W.J. Ding, J. Lindemann, C. Leyens, Materials Chemistry and Physics 118 (2009) 453–458.
[22] H. Mayer, M. Papakyriacou, B. Zettl, S.E. Stanzl-Tschegg, International Journal of Fatigue 25 (2003) 245–256.
[23] D.K. Xu, L. Liu, Y.B. Xu, E.H. Han, Scripta Materialia 56 (2007) 1–4.
[24] T. Morita, M. Shimizu, K. Kawasaki, T. Chiba, Transactions of the JSME 56 (1990) 1915–1922.
[25] M.A. Gharghouri, G.C. Weatherly, J.D. Embury, J. Root, Philosophical Magazine A 79 (1999) 1671–1695.
[26] A.A. Nayeb-Hashemi, J.B. Clark, Metals Park, OH: ASM International, 1988, p. 2520.
[27] D. Chandrasekaran, Materials Science and Engineering A 309–310 (2001) 184–189.
[28] K.Y. Zheng, J. Dong, X.Q. Zeng, W.J. Ding, Materials Science and Engineering A 491 (2008) 103–109.
[29] H. Jin-feng, Y. Hong-yan, L. Yon-bing, C. Hua, H. Jian-ping, Z. Ji-shan, Materials and Design 30 (2009) 440–444.
[30] W.C. Liu, J. Dong, P. Zhang, C.Q. Zhai, W.J. Ding, Materials Transactions 50 (2009) 791–798.